energies

MDPI

Article

A Technique to Optimally Prevent the Voltage and Frequency Violation in Renewable Energy Integrated Microgrids †

Md Asaduzzaman Shoeb [1], Farhad Shahnia [1,*], GM Shafiullah [1] and Fushuan Wen [2]

[1] Discipline of Engineering and Energy, Murdoch University, Perth 6150, Australia; m.shoeb@murdoch.edu.au (M.A.S.); g.shafiullah@murdoch.edu.au (G.S.)
[2] College of Electrical Engineering, Zhejiang University, Hangzhou 310027, China; wenfs@hotmail.com
* Correspondence: f.shahnia@murdoch.edu.au
† A portion of the materials in this paper were previously published (in modified form) in the PhD thesis of the first author at Murdoch University in 2019. This paper is an extension of that work.

Abstract: A microgrid (MG) is always prone to the uncertainties of its demand variation and the generation of its non-dispatchable renewable sources when operating in islanded mode. Such variation events can lead to the voltage or frequency (VF) violation in the MG. However, there are some techniques available in the literature that can predict these events a few minutes ahead. Using such techniques, the VF violation can also be predicted and prevented with the introduction of a suitable preventive controller. Hence, this paper proposes a look-ahead controller that uses the short-horizon prediction data of demand and renewable generation to determine any prospective VF violation. If a violation is predicted, the proposed technique will aim to define the most optimal generation level of dispatchable sources, the MG's best network configuration and the engagement level of the supportive actions, such as exchanging power with neighboring microgrids, utilizing energy storages, a demand response and renewable energy curtailment (if and when available). The technical, reliability and environmental aspects of the MG are considered within the proposed technique along with the operational cost. The determined optimal control variables are then sent to the local controllers to apply the proper arrangements in the system to retain the VF within the desired range. The performance of the developed technique is validated through extensive numerical analyses in MATLAB.

Keywords: microgrid; voltage and frequency management; optimization; preventive control

Citation: Shoeb, M.A.; Shahnia, F.; Shafiullah, G.; Wen, F. A Technique to Optimally Prevent the Voltage and Frequency Violation in Renewable Energy Integrated Microgrids. *Energies* **2023**, *16*, 5774. https://doi.org/10.3390/en16155774

Academic Editor: Ali Mehrizi-Sani

Received: 11 July 2023
Revised: 27 July 2023
Accepted: 1 August 2023
Published: 2 August 2023

1. Introduction

The microgrid (MG) has been a promising approach to proliferate indigenous energy-based distributed generation units (DGs) in the vicinity of end-users. An MG can integrate various renewable-based DGs and energy storages and coordinate them to supply its demand while connected to the main power grid or islanded [1]. Hence, employing standalone MGs is thought of as a significant step in supplying electricity to edge-of-grid and remote areas with limited or no access to utility feeders, while grid-connected MGs can improve the utility's resiliency and reliability [2]. However, the uncertainties of demand and the output power of renewables, along with the high cost of energy storages, complicate the operation of a standalone MG within the desirable range of voltage and/or frequency (VF) in a cost-effective way. Thus, a look-ahead approach that uses the predicted data of such uncertain elements is precious for the MG's optimal performance.

Predicting demand has been an interesting research topic in the field of power systems and distribution networks. Different techniques are proposed in the literature to estimate the demand of a network under different conditions (e.g., day, month or season) [3]. Load-forecasting in an MG is more difficult than in large power systems because a smaller group of loads result in higher randomness [4]. Hence, several approaches have been proposed in

the literature, which has further improved the accuracy of load-forecasting within MGs. As an example, Ref. [4] a hybrid load-forecasting model is suggested, composed of empirical mode decomposition, an extended Kalman filter and particle swarm optimization. A three-stage load-forecasting approach is proposed in [5] that consists of pattern recognition, clustering and multilayer perception. Likewise, Ref. [6] proposes a self-adaptive evolutionary fuzzy model that has a lower load-forecasting error. Such methods are applicable to MGs regardless of their capacity and geographical distribution.

While [4–6] validated their proposals in MGs with large capacities, Ref. [7] proposed another shorter-horizon prediction technique based on a fuzzy algorithm that suits MGs with capacities as low as 20 kW.

Along with the rapid growth of renewables in power systems, there has been increasing research into more accurate forecasting of the variability of renewables, such as wind and solar. A comprehensive review of the different forecasting methods is presented in [8,9]. Various approaches are introduced in [8–13] that can predict the output power of solar and wind systems based on the different scales of the forecast horizon. Data-driven formulations, using historical measurement data, are used in the statistical approaches in [10]. A wind power prediction method and its performance are validated for MGs in [11]. Similarly, Ref. [12] proposed a solar power prediction technique that suits very small-scale photovoltaic systems. Furthermore, Ref. [13] adopted a combination of a sky imager and the neural network to forecast solar energy with 1-second resolutions and 15-minute horizons.

The satisfactory operation of a standalone MG depends on the employed control strategy. Following any changes in the demand or generation of the renewable sources, a fast responding, device-level, local (primary) controller regulates the MG's VF. In addition, an upper-level controller usually coordinates the DGs, by determining the setpoints of their primary controllers. This controller, usually referred to as the MG's central controller (MGCC), is also responsible for maintaining the VF within the desired ranges, by monitoring the system periodically [14]. For example, a fuzzy potential function-based controller is proposed in [15] while [16,17] optimize the droop coefficients of the DGs, based upon the system status and demand, to minimize the fuel cost of the DGs and the power losses. Besides, corrective actions can be employed to bring the VF back into the desired ranges [18]. Such actions in [16–18] take place after detecting VF violation and the new setpoints are transferred to the primary controllers as depicted in Figure 1a. Thus, VF violation will be observed in the MG until the primary controllers act. This time should be shorter than the operation time of the under- and over-VF protective relays, to guarantee their successful operation. This is the key limitation of such corrective techniques.

The state-of-the-art short-horizon prediction approaches can be used at the MGCC to pre-calculate the setpoints of the primary controllers, prior to any potential fierce changes in the uncertain elements. Thus, a controller can be developed that uses prediction tools for predicting the VF violation at T_1 minutes ahead (e.g., 5–15 min depending on the prediction horizon of the utilized forecasting tools), as shown in Figure 1b. This controller can not only avoid the VF violation, but also result in the MG's optimal and improved operation without interfering with the normal operations of the primary or central controllers. This is similar to the proposed methods for large power systems consisting of wind energy in [10] that use a look-ahead cost optimization to decide the unit commitments for two horizons of day-ahead and 5-min ahead. Although the method in [10] considers the expected deviation of predicted data, the sensitivity of the prediction error is unknown. In addition, it only considers the cost of operation without including the VF constraints. Another preventive voltage controller is developed in [19] to improve the short-horizon voltage stability of a large power system. Likewise, Ref. [20] presents a model predictive control-based technique to control the operation of standalone MGs in different time horizons; however, it only focuses on the generation and battery energy storages (BESs) cost and spinning reserve (SR), ignoring the application of demand response (DR) and renewable curtailment (RC). Similarly, Ref. [21] presents a preventive control strategy, which schedules the operation of

the conventional generators in a standalone MG, but only considers the generation cost of the sources.

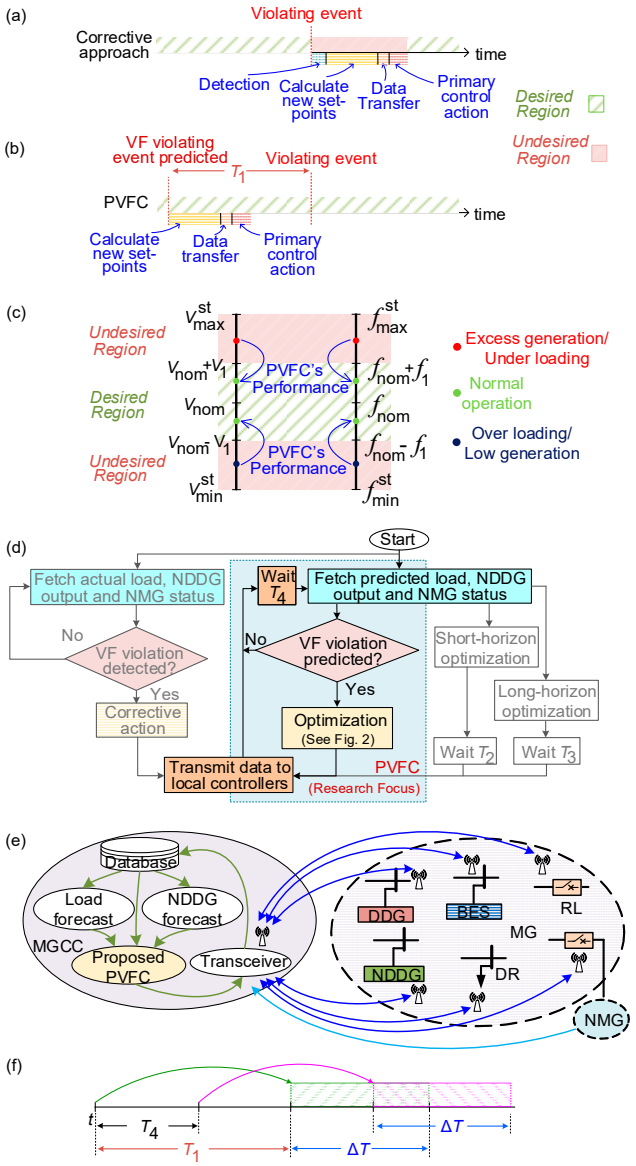

Figure 1. (**a**) VF status when an MG operates with a corrective approach during a violation; (**b**) VF status when an MG operates under the proposed preventive VF controller (PVFC) during a violation; (**c**) *Desired* and *Undesired regions* of VF and the illustration of a successful operation of the proposed PVFC, (**d**) flowchart of MG optimization at various horizons, including the proposed PVFC (the focus of this paper); (**e**) data transmission between the developed PVFC (located within the MGCC) and the various local controllers of MG components; (**f**) PVFC's prediction interval.

Most studies, such as [10,16,17,20,21], have focused on the economic aspects. However, there are other vital criteria, such as the MG's sustainability, emissions, reliability, SR and self-adequacy, that also need to be considered when deciding on its optimal operation. In addition, other supporting technologies, such as DR, RC and network reconfiguration, should be considered and coordinated with BESs. Likewise, the support from the neighboring MGs (NMGs), if available, should be coordinated with the internal supporting technologies (see Appendix A). Moreover, the preventive approaches in [10,20,21] do not investigate the impact of expected/unexpected prediction inaccuracies on system operation. To address these research gaps, this paper presents a preventive VF controller (PVFC) for droop-controlled standalone MGs, which aims to preclude any prospective VF

deviation from the desired range, following changes in the demand and output power of renewables. The proposed technique will be an agent within the MGCC and minimizes the prospective operation cost while maximizing the reliability. It also maintains all the technical constraints (such as SR requirements, the limit of renewable contribution, the line thermal limit and the external dependency of the MG). Minimizing the environmental emissions and power losses in the MG are the other focuses of the technique. To this end, the proposed method uses a multi-objective optimization to determine the optimal dispatch of the DGs (by defining the droop parameters), as well as the contribution level of supportive actions. The supportive measures are the reconfiguration of distribution lines, charging/discharging the BESs and exchanging power with the NMGs, along with managing the level of inessential loads that can be shed or the level of new loads that can be added under the DR, in addition to the amount of RC. The effect of conservative VF reductions on the loads is reflected in the proposed technique by considering the loads' dependency on the VF, while the expected inaccuracies of the predicted data are also taken into account. Table 1 summarizes the considered criteria for the optimization, as well as the assumed control variables within the proposed technique, while comparing them with similar existing techniques (i.e., [10,16,17,20,21]).

Table 1. Comparison of the proposed technique with other existing methods.

		[10]	[16]	[17]	[20]	[21]	This Paper
Control variables	Droop parameters	✘	✔	✔	#	✘	✔
	BES	✘	✘	✘	✔	✔	✔
	DR	✘	✘	✘	✘	✔	✔
	RC	✘	✘	✘	✘	✘	✔
Considered criteria	Operational	✔	✔	✔	✔	✔	✔
	Technical	✘	✘	✘	✔	✘	✔
	Reliability	✘	✘	✘	✔	✘	✔
	Environmental	✘	✘	✘	✘	✘	✔
Suitable for standalone MG		✘	✔	✔	✔	✔	✔
Preventive approach		✔	✘	✘	✔	✔	✔

✔ = True; ✘ = False; # = Not applicable.

The main contributions of the paper to the research field can be summarized as:

- Developing a short-horizon look-ahead PVFC to prevent prospective VF violations following variations in demand or renewables' generation;
- Incorporating technical, reliability and environmental aspects, in addition to the operational costs, in deciding the control variables and coordinating them;
- Considering the impact of the prediction inaccuracy on the outcomes of the control variables within the proposed PVFC.

The remiander of this paper is organized as follows. The concept of the proposed PVFC is discussed in Section 2, while Section 3 presents the formulated problem. The performance of the developed technique is evaluated through several numerical case studies in Section 4. Section 5 discusses the sensitivity of the developed technique. Finally, the key findings of the research are highlighted and summarized in the last section. Five appendices at the end of the paper briefly discuss the idea of provisionally coupled neighboring MGs, the employed optimization solver, the power flow analysis technique, the technical and cost data used in the numerical analyses, the application of PVFC on a large MG and the time complexity of PVFC.

2. The Proposed Technique

Consider an MG consisting of multiple renewable-based non-dispatchable DGs (NDDGs), such as wind or photovoltaic energy, along with some dispatchable DGs (DDGs), such as diesel/gas-based synchronous generators or those renewables that are coupled with an appropriate local power smoothing energy storage. The DDGs are assumed to be droop-controlled and grid-forming, while the NDDGs are thought of as grid-following. The operational principle of the MG, the acceptable range of the VF, the concept of the proposed technique for this MG and its implementation requirements are discussed below.

2.1. Considered Operational Principle of the MG

The VFs at the output of DDGs in the MG are given by the droop equations of [22]

$$f = f^{\max} - m^{\mathrm{DDG}}\, P^{\mathrm{DDG}} \tag{1a}$$

$$V = V^{\max} - n^{\mathrm{DDG}}\, Q^{\mathrm{DDG}} \tag{1b}$$

where P and Q are, respectively, the total active and reactive power injected by the three-phase DDG in kW and kVar, respectively; f and V are the frequency and voltage rms at the output of the DDG in kV and Hz; and $f^{\max}$ and $V^{\max}$ are the VF droop setpoints, while m and n are the P-f and Q-V droop coefficients. It is assumed that the MGCC can adjust $f^{\max}$ and $V^{\max}$, as well as m and n, for every DDG. On the other hand, it is presumed that the output power of the NDDGs can be curtailed if deemed required by the MGCC. The BESs in the MG are assumed to have primary controllers that regulate the active and reactive power transaction at the output of their converters, based on their state of charge. Some of the loads are also thought to operate under the DR program that facilitates shedding non-essential loads or turning on additional loads based on the command signal received from the MGCC. The MG is also presumed to have some reconfigurable lines (RLs), with the help of which the MG's topology can be slightly modified to optimize its operational performance. The MG operator prefers to operate it as a standalone system under normal operating conditions to maintain its autonomy. However, it can be provisionally coupled to suitable NMGs with which it can exchange power (if available) under abnormal conditions (i.e., emergencies, such as overloading or over-generation), as described in Appendix A.

2.2. Desired VF Boundaries

The VF of the MG is preferred to be retained within the *Desired regions* of $V_{\mathrm{nom}} \pm V_1$ and $f_{\mathrm{nom}} \pm f_1$ around the nominal values of V_{nom} and f_{nom} (see Figure 1c). However, due to the variability of the load and NDDGs, the VF may fall in the *Undesired regions* of $V_{\mathrm{nom}} + V_1 \le V \le V^{\mathrm{st}}_{\max}$, $V^{\mathrm{st}}_{\min} \le V \le V_{\mathrm{nom}} - V_1$, $f_{\mathrm{nom}} + f_1 \le f \le f^{\mathrm{st}}_{\max}$ or $f^{\mathrm{st}}_{\min} \le f \le f_{\mathrm{nom}} - f_1$, in which superscript $^{\mathrm{st}}$ denotes the stability margin of VF deviation.

2.3. The Concept

In general, an MG operator has to conduct an economic dispatch for the MG at short horizons of T_2 (e.g., hour, day) and long horizons of T_3 (e.g., month, season, year), as seen from the flowchart of Figure 1d. This is essential for operating the MG optimally [7,20]. Furthermore, corrective actions, such as those proposed in [18], are required after the occurrence of undesired VF in the system to retain the VF within desirable limits, as seen from the operational flowchart of Figure 1d. In contrast to the corrective techniques, the MG operator can further improve its network's optimal performance by using a very short-horizon operational scheme (i.e., even closer to real-time) to consider the sudden changes [23]. To this end, a preventive controller can be employed that analyzes the predicted state of the MG by using the short-horizon prediction data of demand and NDDGs' generation. This technique is an agent within the MGCC and defines the most optimal control variables to prevent any prospective VF violation of the MG. As depicted in Figure 1d,e, those optimal operating settings are then transmitted to the local controllers

of each component to act accordingly. As such, the proposed controller does not replace or adversely affect the long- or short-horizon economic dispatch of the MG. Also, the setpoints, modified by the proposed preventive controller, will be reset to new values, determined under the next short-horizon economic dispatch (see Figure 1d), based on which the MG's VF will be reset to their nominal values.

It should be noted that any state-of-the-art prediction method (such as those proposed in [7,10–13]) can be employed. No specific prediction method has been recommended for the proposed technique, nor does the paper propose a new one. The proposed PVFC is such that the MG operator can employ any available prediction method that has reasonable accuracy. However, considering the unavoidable prediction error, the proposed technique deliberates the estimated mean error of the prediction in deciding the control variables by taking relatively more conservative decisions.

The PVFC will keep looking for any violating events in T_4 intervals ($T_4 < T_1$; e.g., 3-min, see Figure 1d). It will take proactive actions by predicting potential VF violations T_1 minutes ahead for the period of $T_1 < t < T_1 + \Delta T$, as seen schematically from Figure 1f, in which $\Delta T > T_4$ (e.g., 5–15 min).

The PVFC chooses the best resort (i.e., sets of actions that prevent VF violation), including the adjustment of the droop parameters (i.e., different coefficients of m^{DDG} for each DDG and the VF setpoints of $V^{\max}$ and $f^{\max}$ for all DDGs), the on/off status of the switches of each RL, the level of power to be exchanged with available NMGs, the charge/discharge power level of each BES, the RC level of each NDDG and the DR level of loads, based on the costs of the actions.

In this paper, BES's usage is considered more expensive than the cost of power exchange with an NMG, because the frequent charging/discharging of a BES will reduce its life length, and, thus, will increase the imposed cost to the MG operator. Similarly, it is assumed that the hidden costs of RC and DR are more expensive than power exchange with a BES. The PVFC minimizes the overall cost by selecting an optimal combination of actions. This is achieved by solving a non-linear optimization problem.

Mathematical methods, such as dynamic programming, can then be employed to solve this problem. As such problems can have a large number of variables and constraints, solving them efficiently by mathematical methods may be cumbersome. Alternatively, heuristic approaches, such as a modified particle swarm optimization (MPSO), can be employed as suitable solvers. Thus, a constriction factor-based MPSO solver has been chosen in this research (see Appendix B), which has a proven capability to solve non-linear and mixed-integer problems with adequate convergence and stability within a multidimensional space [24,25].

The flowchart of Figure 2 demonstrates the employed stages of the proposed PVFC, which aims at finding the optimal control variables to prevent the MG's VF problem, at the least value of the objective function (OF), which is formulated in Section 3. It first fetches the prediction data of the output power of the NDDGs and loads. Then, it runs a power flow analysis (PFA), adapted for an islanded MG (see Appendix C), to predict the VF. If a VF violation is predicted, it determines the boundaries of the control variables (i.e., the available limits of the resources within the MG). At this point, the MPSO starts to search for the optimal set of control variables and evaluates them. It initializes the random particles and evaluates them by calculating the OF. It keeps on finding the individual best particle and global best particle, followed by updating the velocity and position of particles until it reaches the maximum particle and iteration size.

If less expensive actions can resolve the VF problems, the PVFC will not choose any of the expensive actions. Such a mechanism guarantees that the technique will prevent the VF problem by those actions that are generally low cost (such as adjusting the droop parameters of DDGs) when possible, rather than expensive options (e.g., external power exchange with an NMG or more expensive ones, such as the control of BESs, RC or DR). As the cost of RC and DR are assumed to be very high, it is expected that their contribution will be very limited.

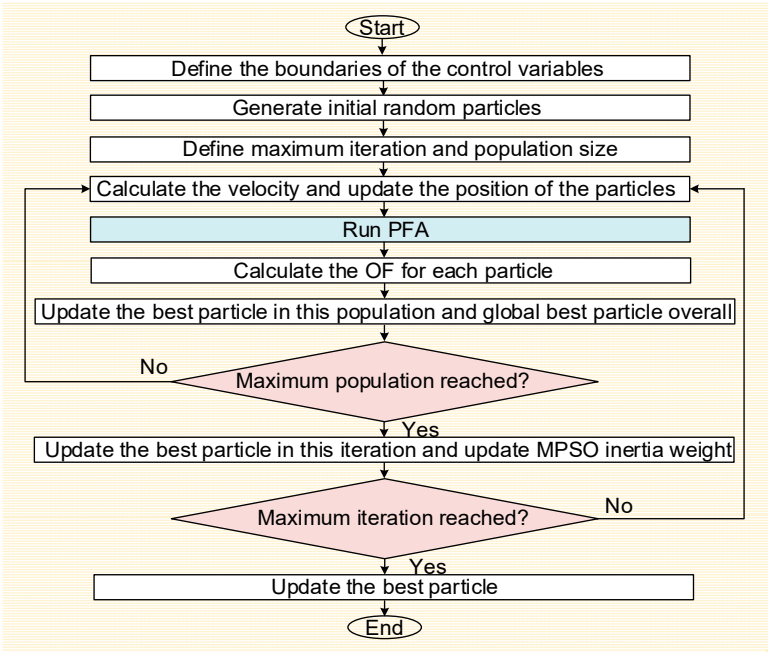

Figure 2. Flowchart of the employed optimization approach within the PVFC.

2.4. Implementation Requirements

For the proposed PVFC, the operation time of the total process to prevent the prospective VF problem must be smaller than T_1. Industrial-level processors and their associated platforms (such as those from National Instruments™ and Intel®) that are currently available in the market can be used to realize the proposed PVFC with an adequate operation time. Also, an IEEE 802.11n-based point-to-multipoint wireless communication system that is currently available on the market [26,27], can be utilized to transmit the determined settings of the control variables to the local controllers of DDGs, NDDGs, BESs, loads and the switches of RLs and switches of NMGs (see Figure 1e). Communication links have high reliability compared to the power system (e.g., an average field-observed mean time before failure of 400 years [28]); however, even if the communication link is broken, as expected from a droop-controlled system, the MG can operate successfully, thanks to the local controllers; however, its operation may be non-optimal.

3. Problem Formulation

The PVFC consists of a mixed-integer non-linear optimization problem with an OF formulated as

$$OF = \sum \pi^s \, OF^s \; \forall s \in \mathbf{S} \tag{2}$$

where

$$OF^s = \omega_1 OF^s_{\text{tech}} + \omega_2 \, OF^s_{\text{op}} + \omega_3 \, OF^s_{\text{sup}} + \omega_4 \, OF^s_{\text{rel}} + \omega_5 \, OF^s_{\text{env}} + Penalty \tag{3}$$

in which

$$OF_{\text{tech}} = VDI + FDI + LLI + SRI + EDI \tag{4a}$$

$$OF_{\text{op}} = C_{\text{gen}} + C_{\text{loss}} \tag{4b}$$

$$OF_{\text{sup}} = C_{\text{trade}} + C_{\text{BES}} + C_{\text{sw}} + C_{\text{DR}} \tag{4c}$$

$$OF_{\text{rel}} = C_{\text{ENS}} \tag{4d}$$

$$OF_{\text{env}} = C_{\text{em}} + C_{\text{RC}} \tag{4e}$$

are the assumed OFs in (3), as illustrated schematically in Figure 3. The considered OFs are derived from the operational needs and expectations of the MG operators. As such, they cover the key aspects of an MG, which are or may be desired by the MG operator when evaluating and improving the performance of the MG (i.e., its technical, operational, reliability and environmental issues).

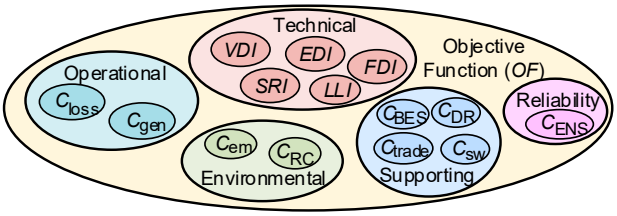

Figure 3. Schematic illustration of different OFs considered in the developed PVFC.

Since the used prediction data may have some inaccuracies, the proposed PVFC assumes multiple scenarios in (2). Considering these scenarios allows the MG operator to take into account the expected accuracy of the prediction of demand and generation of NDDGs. This accuracy is considered in the form of the mean arctangent absolute percentage error (MAAPE) of the predictions, denoted by $\bar{e}$. MAAPE has been specifically chosen as, unlike the percentage error or mean absolute percentage error, it does not yield undefined or infinite values (when considering a parameter with an actual value of zero) [29]. Table 2 lists the assumed scenarios in this study. As seen from (2), each scenario is denoted by s and thought to have a probability of π^s, while **S** is the set representing all scenarios.

Table 2. The assumed scenarios.

s	1	2	3	4	5	6	7	8	9
$\sum P_i^{\text{load}}$	X	$X+\bar{e}$	$X-\bar{e}$	$X+\bar{e}$	$X-\bar{e}$	$X+\bar{e}$	$X-\bar{e}$	X	X
$\sum P_i^{\text{NDDG}}$	Y	$Y+\bar{e}$	$Y-\bar{e}$	$Y-\bar{e}$	$Y+\bar{e}$	Y	Y	$Y+\bar{e}$	$Y-\bar{e}$

X = Predicted amount of demand; Y = Predicted amount of NDDGs' generation; $\bar{e}$ = Prediction MAAPE.

3.1. Technical OF (OF_{tech})

This OF represents the technical aspects of the MG, and is defined by (4a) in which:

- VDI is the voltage deviation index, which determines the maximum voltage deviation across all the buses in the MG. It is derived as

$$VDI = \max(|V_{\text{nom}} - V_i|) \qquad \forall i \in \textbf{BUS} \tag{5}$$

in which the maximum function is denoted by $\max(.)$.

- FDI is the frequency deviation index, representing the deviation of the MG's frequency from the nominal value, as defined by

$$FDI = |f_{\text{nom}} - f| \tag{6}$$

- LLI is the MG's lines loading index and allows the line currents temporarily to exceed the maximum limit in the case of an emergency (if required). It is derived by

$$LLI = \begin{cases} \left|1 - \frac{I_i}{I_i^{\max}}\right| & \exists\, I_i > I_i^{\max} \\ 0 & \text{otherwise} \end{cases} \qquad \forall i \in \textbf{LINE} \tag{7}$$

where I represents current and **Line** is the set representing all the distribution lines in the MG.

- SR expresses the unused percentage of the capacity of the MG's energized rotary DDGs. Maximizing the SR is crucial to improving the dynamic response of the MG, following an unexpected and rapid variation in the generation of its NDDGs or the consumption of its loads. To this end, the SR index, denoted by SRI, is derived by

$$SRI = \frac{\sum P_i^{\mathrm{DDG}}}{\sum \left(P_i^{\mathrm{DDG}}\right)^{\max}} \qquad \forall i \in \mathrm{ROT} - \mathrm{DDG} \tag{8}$$

  in which $\mathrm{ROT} - \mathrm{DDG}$ is the set representing the energized rotary DDGs. As such, the total power generated by these DDGs will reduce; however, this reduction does not aim to reduce these DDGs' generation costs but looks to maximize the MG's SR.
- EDI denotes the MG's dependency index on the external NMG, formulated as

$$EDI = \frac{\sum \left|S_i^{\mathrm{ex}}\right|}{\sum S_j^{\mathrm{load}}} \qquad \forall i \in \mathbf{NMG},\ \forall j \in \mathbf{LOAD} \tag{9}$$

  where S^{ex} and S^{load} are, respectively, the apparent power that the MG exchanges with NMGs and that is consumed by the MG's loads, while **NMG** and **LOAD** are, respectively, the sets representing all the NMGs with whom the MG is exchanging power and load points.

3.2. Operational OF (OF_{op})

The second parameter in (3), represents the MG's operational cost and is defined by (4b) in which C_{gen} is the power generation cost by DGs and C_{loss} is the cost corresponding to power losses in MG lines. C_{gen} is calculated as

$$C_{\mathrm{gen}} = \sum \left(P_i^{\mathrm{DG}}\ fuel_i\ C_i^{\mathrm{fuel}} + C_i^{\mathrm{O\&M}} + C_i^{\mathrm{life}} \right) \Delta T + C_i^{\mathrm{start}} \qquad \forall i \in \mathbf{DG} \tag{10}$$

in which **DG** is the set representing all DGs of the MG and P^{DG} is the output power of a DG over the period of ΔT (in h) while $fuel$ and C^{fuel} are, respectively, its fuel consumption (in L/kWh) and corresponding cost (in \$/L). $C^{\mathrm{O\&M}}$ denotes its operation and maintenance cost (in \$/h). C^{life} is the life-loss cost of the DG, formulated as

$$C_i^{\mathrm{life}} = \left(C_{\mathrm{cap}}^{\mathrm{DG}}\right)_i / T_i^{\mathrm{op}} \tag{11}$$

in which T^{op} and $C_{\mathrm{cap}}^{\mathrm{DG}}$ are, respectively, the total operation lifetime of the DG (in h) and its capital cost (in \$). C_i^{start}, in (10), is the cost to start up a DG, formulated as

$$C_i^{\mathrm{start}} = Cost_i^{\mathrm{ST}} x_i \tag{12}$$

in which $Cost_i^{\mathrm{ST}}$ is the starting-up cost of a DG while x is a binary variable equal to 1 if a DG starts up and 0 otherwise.

C_{loss} is defined as

$$C_{\mathrm{loss}} = P_{\mathrm{loss}}\ Cost^{\mathrm{loss}}\ \Delta T \tag{13}$$

where P_{loss} is the total power loss in the MG's lines (in kW) while $Cost^{\mathrm{loss}}$ denotes the associated cost (in \$/kWh). It should be noted that the P^{DDG}, P_{loss} and f of the MG are calculated from the employed PFA.

3.3. Supportive OF (OF_{sup})

This OF is defined by (4c) and represents the cost of the supportive actions, such as exchanging power with NMGs, charging/discharging BESs, switching on/off the RLs and DR, in which:

- C_{trade} is MG's net energy trading cost with its NMGs, defined from

$$C_{\text{trade}} = \left(\sum \left|(P_i^{\text{ex}})^{\text{imp}}\right| \left(Cost_i^{\text{trade}}\right)^{\text{imp}} - \left|(P_i^{\text{ex}})^{\text{exp}}\right| \left(Cost_i^{\text{trade}}\right)^{\text{exp}}\right) \Delta T \qquad \forall i \in \textbf{NMG} \tag{14}$$

in which it is an expense when an MG is importing power, while it is an income when exporting. $Cost^{\text{trade}}$ is the traded power's unit cost (in \$/kWh), which is assumed to be the same for exporting and importing; however, in general, they can be different.

- C_{BES} is the life-loss cost of BESs, derived as [30,31]

$$C_{\text{BES}} = \sum \frac{\left(C_{\text{cap}}^{\text{BES}}\right)_i \lambda_i \, P_i^{\text{BES}}}{E_i^{\text{life}}} \Delta T \qquad \forall i \in \textbf{BES} \tag{15}$$

in which the charging/discharging power of a BES (in kW), its total cumulative throughput in its life cycle (in kWh) and its capital cost (in \$/kWh) are, respectively, denoted by P^{BES}, E^{life} and $C_{\text{cap}}^{\text{BES}}$. The parameter λ is used in (15) to consider the impact of the BES's state of charge, according to [30]. The set of BESs are represented by **BES**.

- C_{sw} is the cost incurred from switching RLs, calculated from

$$C_{\text{sw}} = N_{\text{sw}} \, Cost^{\text{sw}} \tag{16}$$

where N_{sw} and $Cost^{\text{sw}}$ are, respectively, the total number of switchings (i.e., connecting/disconnecting a RL), and their corresponding cost (in \$/switching). In this research, it is assumed that the connection/disconnection of a RL involves the closing/opening of two switches, at its ends.

- C_{DR} is the cost of controlling loads under DR, determined from

$$C_{\text{DR}} = \sum \left(\Delta P_i^{\text{DR}}\right)^{\text{shed}} \left(Cost_i^{\text{DR}}\right)^{\text{shed}} + \sum \left(\Delta P_j^{\text{DR}}\right)^{\text{add}} \left(Cost_j^{\text{DR}}\right)^{\text{add}} \qquad \forall i, j \in \textbf{DR} \tag{17}$$

where **DR** is the set representing those loads of the MG with the DR feature; ΔP^{DR} is the amount of loads modified under the DR (in kW) in which the superscripts $^{\text{shed}}$ and $^{\text{add}}$, respectively, denote those inessential loads that have been shed or the additional loads that are turned on, while $Cost^{\text{DR}}$ represents the corresponding costs (in \$/kWh).

3.4. Reliability OF (OF_{rel})

This OF considers the reliability of the resources of the MG and is formulated in (4d), where C_{ENS} is the cost of energy not supplied, and is defined as

$$C_{\text{ENS}} = ENS \; Cost^{\text{ENS}} \; \Delta T \tag{18}$$

where ENS shows the energy not supplied (in kW) and is derived in (19) using the given availability (Av) of DGs, BESs and NMGs. $Cost^{\text{ENS}}$ is the cost of ENS (in \$/kWh) [32].

$$ENS = \sum (1 - Av_i) \; |P_i| \qquad \forall i \in \textbf{\textit{DG}}, \; \textbf{\textit{BES}}, \; \textbf{\textit{NMG}} \tag{19}$$

3.5. Environmental OF (OF_{env})

This OF considers the environmental aspects in terms of the emissions incurred from the DGs and RC as depicted in (4e).

The cost of emissions is denoted by C_{em} and is derived by

$$C_{\text{em}} = \sum P_i^{\text{DG}} \; Em_i^{\text{DG}} \; Cost^{\text{em}} \; \Delta T \qquad \forall i \in \textbf{DG} \tag{20}$$

where Em^{DG} and $Cost^{\text{em}}$, respectively, the emission level of a DG for electricity generation (in kg/kWh) and its corresponding cost (in \$/kg), are constant values that can be deter-

mined from the generator specifications and emissions policy [33]. The cost of RC, C_{RC}, is defined by

$$C_{RC} = \sum \Delta P_i^{RC} Cost_i^{RC} \Delta T \qquad \forall i \in \text{NDDG} \tag{21}$$

where ΔP^{RC} and $Cost^{RC}$ are, respectively, the level of RC (in kW) and its associated cost (in \$/kWh) while **NDDG** denotes the set of NDDGs.

Table 3 summarizes the factors affecting some of the above costs and provides exemplary values for them, as provided in the literature.

Table 3. Considered costs in the formulated OF and the factors affecting them.

Costs	Impacted by	Exemplary Value
$Cost^{DR}$	Fitting cost of DR technologies, financial incentives for the customer, power usage profile of the customer, the estimated energy shifted by DR annually.	1–20 \$/kWh [34]
$Cost^{em}$	Plausible cost of public and environmental damage, the projected amount of emissions.	0.02–0.09 \$/kg [35]
$Cost^{ENS}$	Projected interruption duration and frequency, the non-utilized investment cost of equipment, the penalty paid to the customer.	1–50 \$/kWh [36]
$Cost^{loss}$	The investment cost of network installation, cost of energy sold to consumers, maximum annual power loss.	0.04 \$/kWh [37]
$Cost^{O\&M}$	Necessary maintenance and total operation hours.	0.03 \$/h [38]
$Cost^{RC}$	Non-utilized capital cost of NDDGs, lost income due to curtailing the harnessable energy, the estimated annual amount of curtailed energy.	0.5–20 \$/kWh [39]
$Cost^{SW}$	Investment and maintenance cost of the switch, the estimated number of actions.	0.25 \$/switching

3.6. Technical Constraints

The aim of the solver is to find a set of control variables (see Figure 3) that minimizes the OF of (2) subject to the technical constraints of

$$\sum S_{k_1}^{DG} + \sum \beta S_{k_2}^{BES} + \sum \gamma S_{k_3}^{NMG} = \sum S_{k_4}^{load} + S^{loss} \tag{22a}$$

$$|\Delta V_i| \leq |\Delta V|^{max} \qquad \forall i \in \textbf{BUS} \tag{22b}$$

$$|\Delta f| \leq \Delta f^{max} \tag{22c}$$

$$I_i \leq I_i^{max} \qquad \forall i \in \textbf{LINE} \tag{22d}$$

$$SRI \leq SRI^{max} \tag{22e}$$

$$EDI \leq EDI^{max} \tag{22f}$$

$$RCI \leq RCI^{max} \tag{22g}$$

$$P_{loss} \leq P_{loss}^{max} \tag{22h}$$

$$\alpha_i^{DDG} \left(P_i^{DDG}\right)^{max} \leq P_i^{DDG} \leq \left(P_i^{DDG}\right)^{max} \forall i \in \text{DDG} \tag{22i}$$

$$\begin{cases} P^{\mathrm{DDG}} = 0 & \text{if } t^{\mathrm{off}}_{\mathrm{DDG}} < (T_{\mathrm{DDG}})^{\mathrm{off}} \\ P^{\mathrm{DDG}} > 0 & \text{if } t^{\mathrm{on}}_{\mathrm{DDG}} < (T_{\mathrm{DDG}})^{\mathrm{on}} \end{cases} \tag{22j}$$

$$\left| P^{\mathrm{DDG}}_{t} - P^{\mathrm{DDG}}_{t-\Delta t} \right| \leq \begin{cases} \left(RR^{\max}_{\mathrm{DDG}}\right)^{\mathrm{up}} & \text{if } P^{\mathrm{DDG}}_{t} > P^{\mathrm{DDG}}_{t-\Delta t} \\ \left(RR^{\max}_{\mathrm{DDG}}\right)^{\mathrm{down}} & \text{if } P^{\mathrm{DDG}}_{t} < P^{\mathrm{DDG}}_{t-\Delta t} \end{cases} \tag{22k}$$

Equation (22a) presents the active and reactive power balance constraints within the MG in which β for every BES is, respectively, +1 and -1 when it is discharging and charging and γ for each NMG +1 and -1, respectively, when it is exporting power to and importing from the MG. Equations (22b) and (22c) show the maximum allowed deviations of frequency (Δf) and voltage magnitude ($|\Delta V|$) at all buses of the MG and (22d) represents the maximum thermal limits of its lines when conducting a current. Equation (22e) defines the MG's maximum limit of SRI while (22f) defines the MG's maximum acceptable dependency on the NMGs. On occasion, the operators often wish to limit the contribution of the non-dispatchable renewable sources, which can be realized by the constraint in (22g). Here, the renewable contribution index, RCI, is defined as the ratio of the total contribution of NDDGs and BESs to the total supplied load as derived by

$$RCI = \frac{\sum P^{\mathrm{NDDG}}_{i} + \sum P^{\mathrm{BES}}_{j}}{\sum P^{\mathrm{load}}_{k}} \qquad \forall i \in \mathrm{NDDG},\ \forall j \in \mathrm{BES},\ \forall k \in \textbf{LOAD} \tag{23}$$

whereas the maximum allowable loss is set at (22h). The dispatching constraints of DDGs (i.e., their minimum loading, minimum downtime, minimum uptime, maximum ramp-up rate and maximum ramp-down rate) are given in (22i–k), in which α_{DDG} is the percentage of minimum loading of a DDG based on its efficiency constraints (defined in the manufacturer's specifications); $(T_{\mathrm{DDG}})^{\mathrm{off}}$ and $(T_{\mathrm{DDG}})^{\mathrm{on}}$ denote, respectively, the required time for a DDG that cannot turn on once it is turned off and the required time that it has to operate after turning on and $RR^{\max}_{\mathrm{DDG}}$ represents the maximum ramping-up/down rate of a DDG [40]. It is worth noting that DDGs may include both rotating and converter-based DGs. Hence, the parameters of T_{DDG} and $RR^{\max}_{\mathrm{DDG}}$ can be different from one DDG to another based on their type and operating principles. It is worth noting that the proposed technique is not bound to any specific network topology (e.g., radial, loop, mesh). In (22), the superscript max denotes the maximum allowable limit.

In (3), *Penalty* is used to eliminate those sets of actions that violate any of the constraints in (22) and it is defined as

$$Penalty = \begin{cases} 10^{6} & \text{if (7) is unsatisfied} \\ 0 & \text{otherwise} \end{cases} \tag{24}$$

3.7. Control Variable Boundaries

Figure 4 illustrates the considered MPSO particle containing the control variables while their boundaries (if applicable) are given in (25), in which the charging and discharging active power limit of the BES and its converter's reactive power exchange limit are denoted by (25a,b), where S^{BES} is the apparent power of the BES's converter. The maximum allowed limit of exchanging active and reactive power with the NMGs is defined in (25c,d). The boundary of RC is defined in (25e), in which α^{RC} is the allowable percentage of renewables that can be curtailed. The allowed range of load shedding and turning on additional loads under DR are presented by (25f,g), denoted, respectively, by α^{shed} and α^{add}, in which $\left(P^{\mathrm{load}}\right)^{\mathrm{shed}}$ and $\left(P^{\mathrm{load}}\right)^{\mathrm{add}}$ are the capacity of load shedding and turning on additional loads. In (25), the superscript $^{\max}$ denotes the maximum allowable limit.

$$-\left(P^{\mathrm{charge}}_{i}\right)^{\max} \leq P^{\mathrm{BES}}_{i} \leq \left(P^{\mathrm{discharge}}_{i}\right)^{\max} \qquad \forall i \in \textbf{BES} \tag{25a}$$

$$-\sqrt{\left(S_i^{\mathrm{BES}}\right)^2-\left(P_i^{\mathrm{BES}}\right)^2} \le Q_i^{\mathrm{BES}} \le \sqrt{\left(S_i^{\mathrm{BES}}\right)^2-\left(P_i^{\mathrm{BES}}\right)^2} \quad \forall i \in \mathbf{BES} \tag{25b}$$

$$-\left(P_i^{\mathrm{imp}}\right)^{\max} \le P_i^{\mathrm{ex}} \le \left(P_i^{\mathrm{exp}}\right)^{\max} \quad \forall i \in \mathbf{NMG} \tag{25c}$$

$$-\sqrt{\left(S_i^{\mathrm{ex}}\right)^2-\left(P_i^{\mathrm{ex}}\right)^2} \le Q_i^{\mathrm{ex}} \le \sqrt{\left(S_i^{\mathrm{ex}}\right)^2-\left(P_i^{\mathrm{ex}}\right)^2} \quad \forall i \in \mathbf{NMG} \tag{25d}$$

$$0 \le \Delta P_i^{\mathrm{RC}} \le \alpha^{\mathrm{RC}} P_i^{\mathrm{NDDG}} \quad \forall i \in \mathbf{NDDG} \tag{25e}$$

$$0 \le \left(\Delta P_i^{\mathrm{DR}}\right)^{\mathrm{shed}} \le \alpha^{\mathrm{shed}} \left(P_i^{\mathrm{load}}\right)^{\mathrm{shed}} \quad \forall i \in \mathbf{DR} \tag{25f}$$

$$0 \le \left(\Delta P_i^{\mathrm{DR}}\right)^{\mathrm{add}} \le \alpha^{\mathrm{add}} \left(P_i^{\mathrm{load}}\right)^{\mathrm{add}} \quad \forall i \in \mathbf{DR} \tag{25g}$$

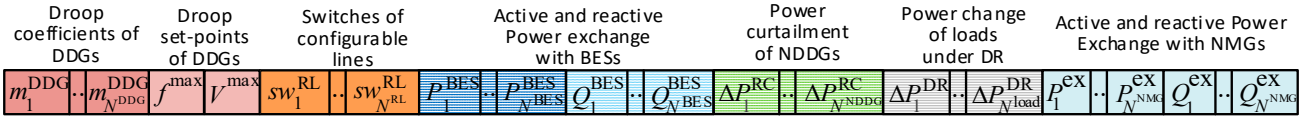

Figure 4. Schematic illustration of the considered particle for the MPSO composed of assumed control variables.

3.8. Weightings

It should be highlighted that the weightings of ω_1 to ω_5 ($\sum \omega_i = 1$) in (3) are the corresponding weightings of the assumed OFs and reflect the importance of each criterion. Since there is no mathematical approach to define them for complex systems and real-world problems, like electrical systems, an acceptable method is a census from the experts or MG operators and using their experience and outlook [41].

4. Performance Evaluation

Consider the 10-bus system of Figure 5, which has been extracted from [42] and modified to evaluate the performance of the proposed PVFC. This MG consists of two NDDGs, three DDGs, two BESs, two RLs and one connection to an NMG (through bus-7), supplying a maximum demand of 20 kVA. NDDG-1 and 2 are thought of as small-scale converter-based wind turbine and photovoltaic systems, respectively, operating under maximum power point tracking. DDG-1 and DDG-2 are assumed, respectively, to be biomass and diesel-driven generators, while DDG-3 is considered to be a solar-driven, converter-based DG (with a suitably sized local power smoothing storage that makes it dispatchable). Hence, DDG-1 and DDG-3 are the renewable-based DDGs. These DDGs are assumed to have equal ratings of 10 kVA (and a maximum active power supply capacity of 7 kW, see Table A1 in Appendix D) [43]. It should be noted that an equal rating does not mean equal load sharing, as their power generation is determined by their droop coefficients (i.e., m_1, m_2 and m_3), defined by the proposed controller. As such, regardless of their ratings, they can share the loads equally or unequally.

The *Desired regions* of VF for the MG are assumed as 1 ± 0.05 per-unit (pu) and 50 ± 0.5 Hz, while $V_{\max}^{\mathrm{st}} = 1.1$ pu, $V_{\min}^{\mathrm{st}} = 0.9$ pu, $f_{\max}^{\mathrm{st}} = 51$ Hz and $f_{\min}^{\mathrm{st}} = 49$ Hz. The forecast horizon and the prediction interval are, respectively, $T_1 = 5$ and $T_4 = 3$ min, while the predicted data have 1-min resolutions. It is also presumed that all scenarios in Table 2 have the same probability (i.e., $\pi^1 = \ldots = \pi^9$) while $\bar{e} = 15\%$. The impact of π^S and $\bar{e}$ are discussed through a sensitivity analysis in the following section. Appendix D provides the considered technical parameters in modeling this MG, as well as the introduced costs

in Section 3, along with the assumed values for the weightings of ω_1 to ω_5 and the base values of voltage, power and frequency for the numerical analyses.

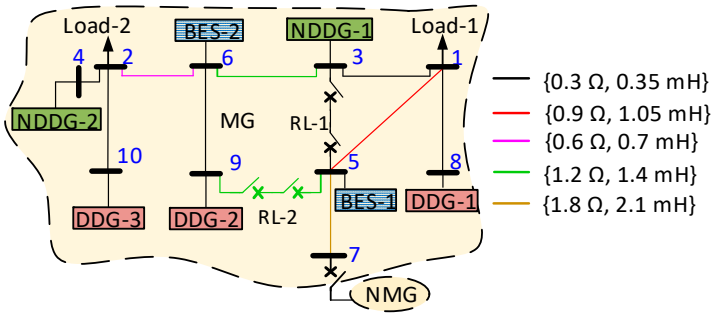

Figure 5. Considered MG system for the numerical analyses.

It should be noted that the proposed PVFC can be employed in standalone MGs, regardless of the network's voltage level (i.e., low or medium voltage), the network's topology (e.g., radial, loop, mesh) or the number of load/generator buses. This is demonstrated in Appendix E, which shows a medium voltage large MG.

4.1. Sample Performance

Let us first envisage the operation of the considered MG over a sample 60-min period with the assumed variations in its demand and NDDGs, as shown in Figure 6a. As seen in Figure 6b,c, at t = 13 min, a frequency rise beyond the *Desired region* is forecasted for t = 18 min. Therefore, the PVFC activates promptly to prevent the prospective frequency deviation. It modifies the droop coefficients of the DDGs to a new optimal level (see Figure 6d) to reduce the output power of DDG-2 and DDG-3. The frequency droop setpoint of $f^{\max}$ is also slightly reduced (see Figure 6e). As such, the VF is retained within the *Desired region* (see Figure 6b,c). At t = 28 min, an increase in demand and a drop in the NDDG's power are forecasted for t = 33 min, which would result in a VF drop beyond the *Desired region* (see Figure 6b,c). To prevent this, the PVFC adjusts the power dispatch from the DDGs to new optimal levels by changing their corresponding droop coefficients while increasing the VF droop setpoints (see Figure 6d,e). However, these actions are not enough to prevent the *Undesired region* operation. A power of 0.015 pu has also to be imported from the NMG (as depicted in Figure 6f). The PVFC does not choose to request support from expensive actions, such as exchanging power with the BESs, DR or RC in these instances. PVFC also keep *SRI*, *RCI* and *EDI* indices below the allowed levels, as depicted in Figure 6g–i. The real operating cost (ROC) of the MG (the accumulated cost of the fuel consumption, emissions and maintenance of DDGs, as well as the cost of power trading with the NMG and the cost of DR) before implementing the proposed PVFC and after that are presented in Figure 6j for the same period. It can be seen from this figure that the proposed PVFC has also reduced the ROC of the MG for the majority of that period. The above example illustrates the effectiveness of the PVFC in retaining the VF of the MG within the *Desired region* at the least cost.

To demonstrate the capability of the proposed PVFC in improving the MG's performance along with controlling the VF, let us consider the predicted event at t = 33 min in which the PVFC prevents a prospective undesired VF violation. To this end, it rearranges the dispatch of the DDGs by increasing the contribution of the DDG-1 and DDG-3 (see Figure 7a), which are closer to the load buses. At the same time, it also finds importing 5% of the demand from the available NMG is required to support the MG, since this power is assumed to be cheaper than other supportive actions (as seen from Table A1 in Appendix D). The expensive diesel-based DDG-2 supplies 9% less power according to the PVFC's decision to reduce the operational and emissions costs while improving the MG's SR (i.e., reducing the *SRI*). Figure 7b illustrates the percentage improvements of each OF of (3) and the MG's ROC under the proposed PVFC versus the condition when the PVFC

is not implemented. It can be seen from this figure that by applying the defined control variables of the PVFC, OF_{tech} and OF_{op} reduce by 10%, and the MG's emissions reduce by almost 30% while OF_{rel} improves slightly, and the MG's ROC reduces by 2%.

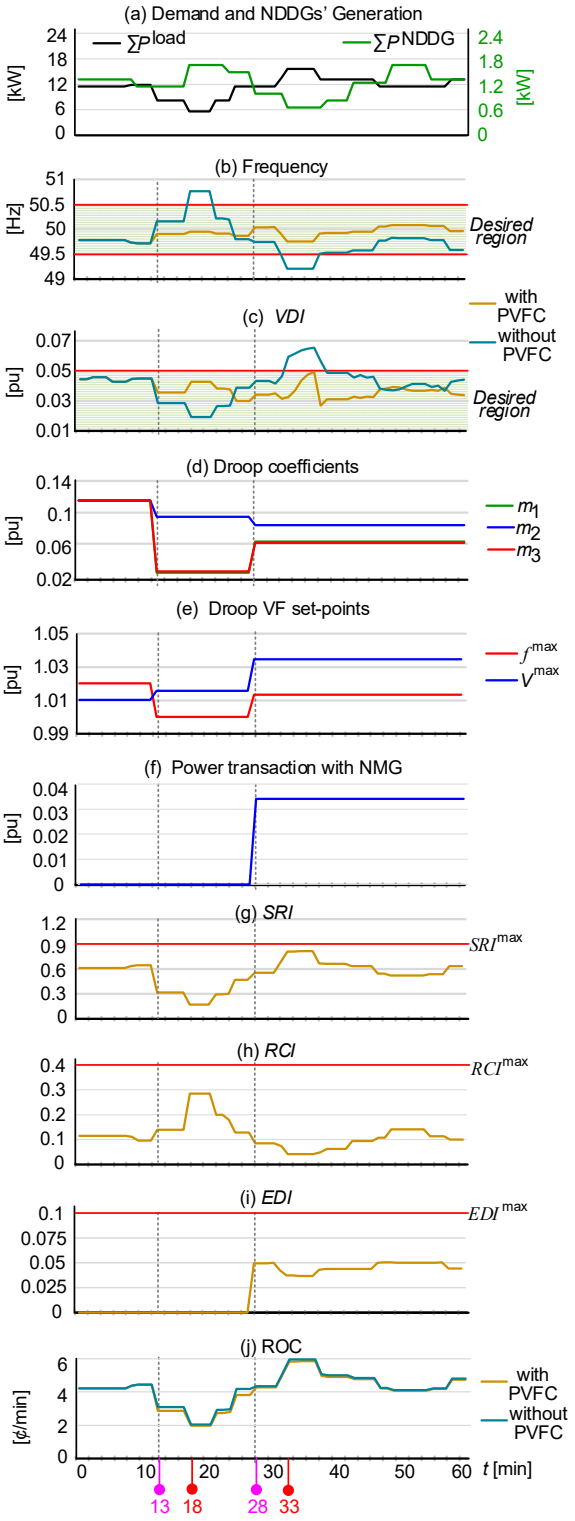

Figure 6. (**a**) Variation in demand and NDDGs' output power; (**b**) MG's frequency with and without the proposed PVFC; (**c**) MG's VDI with and without the proposed PVFC; (**d**) droop coefficients of DDGs; (**e**) droop setpoints of DDGs; (**f**) power transaction between MG and NMGs; (**g**) MG's SRI; (**h**) MG's RCI; (**i**) MG's EDI; (**j**) MG's ROC with and without the proposed PVFC.

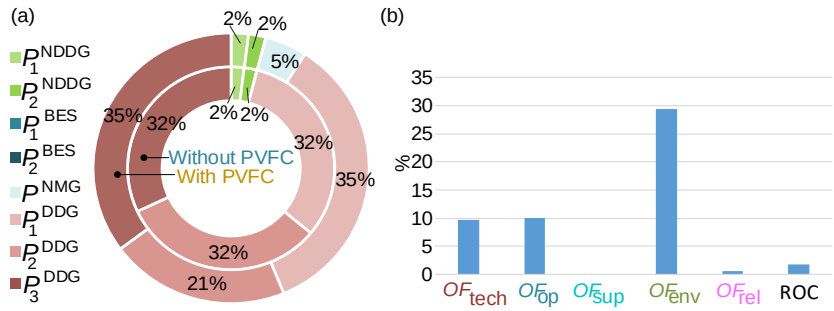

Figure 7. (**a**) Individual contribution of different elements of the MG to retain VF within the *Desired region*; (**b**) percentage improvements of OFs and ROC because of PVFC.

4.2. Performance under Prediction Errors

The proposed PVFC uses the data from forecasting tools. Even though $\bar{e}$ is considered in formulating the problem (see Table 2), the actual prediction error (e) can be larger or smaller than $\bar{e}$ [44]. To visualize the impact of $e \neq \bar{e}$, on the operation outcome of the proposed PVFC, another study is conducted. In this study, it is assumed that the real demand or generation by NDDGs has a small difference (below 15%) from those predicted amounts, which is aligned with the accuracies reported in [3,6]. Figure 8 illustrates eight sample cases with a small e. Case-1 considers four instances where the actual value of load/NDDG power is lower than the predicted values, while Case-2 considers another four instances in which the actual values are beyond the predicted values. The predicted values and the observed actual values for these eight cases are summarized in Table 4.

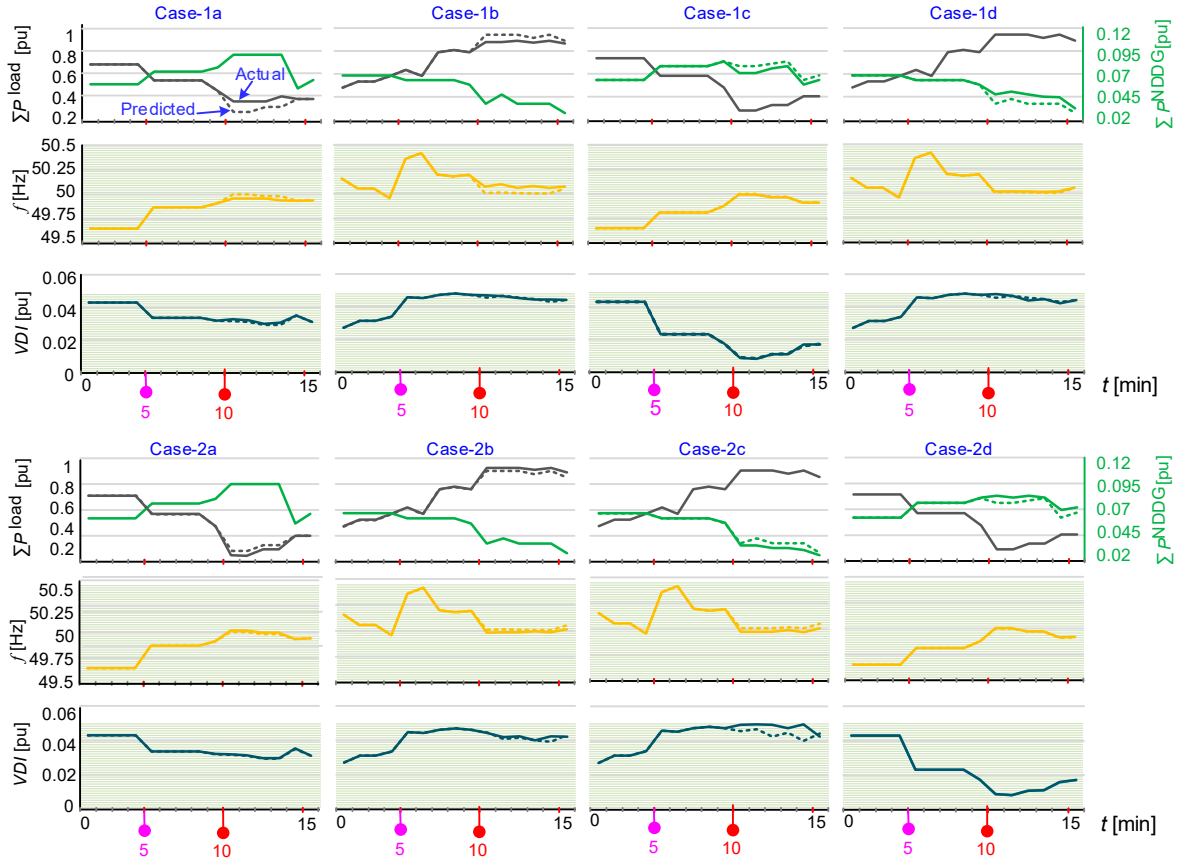

Figure 8. The actual and predicted demand, NDDGs' generation and the resulting frequency and *VDI* under the proposed PVFC for the assumed study cases in Table 4.

Table 4. The assumed prediction and actual amount of the total demand and NDDGs' generation change between t = 5 and 10 min.

	Case-	**1a**	**1b**	**1c**	**1d**	**2a**	**2b**	**2c**	**2d**
$\sum P_i^{\text{load}}$	Initial (pu)	0.57	0.62	0.57	0.62	0.57	0.62	0.57	0.62
	Prediction (%)	−50	+46	−50	+46	−50	+46	−50	+46
	Actual (%)	−35	+37	−50	+46	−56	+50	−50	+46
$\sum P_i^{\text{NDDG}}$	Initial (pu)	0.08	0.06	0.08	0.06	0.08	0.06	0.06	0.08
	Prediction (%)	25	−38	0	−38	25	−38	−38	0
	Actual (%)	25	−38	−9	−23	25	38	−42	+9

In Case-1a, at t = 5 min, a demand decrease of 50% is predicted for t = 10 min, which will lead to a frequency rise beyond the *Desired region*. Thus, the PVFC is activated and optimizes the control variables. However, at t = 10 min, the observed actual demand is found to be 15% higher than the predicted demand (i.e., $e = 15\%$). However, the VF within the MG stays within the *Desired region* (see Figure 8-1a). In Case-1b, an overloading was predicted, which indicated a prospective VF drop beyond the *Desired region*; however, in reality, the actual demand observed is found to be 9% lower than the predicted amount (i.e., $e = -9\%$). Therefore, the MG's frequency is slightly higher than the predicted amount but still within the *Desired region* while the voltage deviation is not affected much (see Figure 8-1b). Similarly, Case-1c and d represent, respectively, instances in which an e of 9 and 15% are observed in the generation amount of NDDGs. However, in both cases, the VF of the MG are hardly impacted by this prediction error (see Figure 8-1c,-1d).

Case-2a represents a scenario in which the actual demand drops 6% more than the predicted amount (i.e., $e = 6\%$). However, the MG operates without any unacceptable VF deviation with the help of the proposed PVFC (see Figure 8-2a). Case-2b shows an instance in which the actual demand rises 4% more than the predicted amount (i.e., $e = 4\%$); however, it is found that the inaccuracy has very little effect on the MG's VF (see Figure 8-2b). Conversely, Case-2c depicts a scenario in which the actual NDDG power is 4% lower than the predicted amount (i.e., $e = 4\%$). As a result, the frequency drops slightly, and the voltage deviation increases, but both are within the *Desired region* (see Figure 8-2c). In Case-2d, the actual NDDGs' generation is 9% higher than the predicted amount (i.e., $e = 9\%$). However, this inaccuracy does not result in any deviance in the VF (see Figure 8-2d).

4.3. Comparative Analysis

As depicted in Table 1, there are limited works that can be numerically compared with the proposed PVFC. The overloading event at t = 33 min of the example of Section 4.1 is re-analyzed by the methods of [16,21] to demonstrate a comparative analysis against the proposed PVFC. The results are summarized in Table 5, which lists VDI, FDI, ROC and line losses along with the values of different OFs of (3). The study shows that the proposed PVFC has, respectively, 45% and 51% better VDI than [16,21]. Likewise, a better outcome is seen for most of the parameters while for a few (i.e., ROC, FDI, OF_{tech}, OF_{rel}), an almost similar performance is observed (as depicted in Table 5). Additionally, several other events were analyzed as part of this study in which the existing techniques failed to maintain the VF while the proposed PVFC was successful.

Table 5. Comparative analysis of the proposed PVFC against the methods proposed in [16,21] for an overloaded event.

Parameters	**[16]**	**[21]**	**This Paper**
VDI (pu)	0.048 (+45%)	0.0498 (+51%)	0.033
FDI (Hz)	0.5 (0%)	0.5 (0%)	0.5
ROC (¢/min)	5.72 (−1.38%)	5.74 (−1%)	5.8
P_{loss} (kW)	0.94 (+9.3%)	0.94 (9.3%)	0.86
OF_{tech}	0.93 (0%)	0.92 (−1%)	0.93
OF_{op}	1.75 (+7.4%)	1.74 (+6.7%)	1.63
OF_{rel}	16.78 (+2%)	16.75 (+1.8%)	16.46
OF_{env}	3.32×10^{-4} (+17.7%)	3.32×10^{-4} (+17.7%)	2.82×10^{-4}

5. Sensitivity Analysis

As seen from the previous section, e can affect the OFs and the MG's ROC. On the other hand, the considered $\bar{e}$ and π^S, in Table 2, also affect the outcome of the PVFC. Hence, this section discusses the sensitivity of PVFC regarding these parameters.

5.1. Actual Prediction Error (e)

Consider the predicted event at t =18 min of the example of Section 4.1. The PVFC finds that the VF of the MG can be retained within the *Desired region* by only rearranging the dispatch of the DDGs (through optimally adjusting the droop coefficients of the DDGs). A sensitivity analysis is conducted in which the actual demand varies from –15 to +15% in steps of 5%, from the predicted value. The actual value of each of the OFs in (3) is calculated using the defined control variables by the PVFC (assuming $\bar{e} = 0$).

Figure 9a illustrates the percentage change of OFs as e increases from –15 to +15% and shows this linear relationship. Figure 9b illustrates the expected amount of each of these Ofs and the ROC, along with the range of their variation within the assumed error range, while Figure 9c depicts the range of the control variables (i.e., the droop coefficients of the DDGs) for each actual demand level by re-analyzing the MG for each actual demand. Figure 9b shows that the predicted ROC is 2.6 ¢/min; however, it increases to 3 ¢/min when the actual demand is 15% higher than the predicted amount (i.e., e = +15%) while it drops to 2.2 ¢/min when the actual demand is 15% below the prediction (i.e., $e = -15\%$). Table 6 lists the correlation index of these OFs and the MG's ROC with e and demonstrates a positive and linear correlation for all parameters with an index of 0.99.

Table 6. Correlation indices among the variety of different OFs and MG's ROC versus the variations in e, $\bar{e}$ and π^1.

Parameters	e	$\bar{e}$	π^1
OF_{tech}	0.99	−0.99	0.58
OF_{op}	0.99	−0.99	−0.92
OF_{sup}	0.99	0.99	−0.62
OF_{rel}	0.99	−0.99	−0.96
OF_{env}	0.99	−0.99	0.14
ROC	0.99	0.99	−0.40

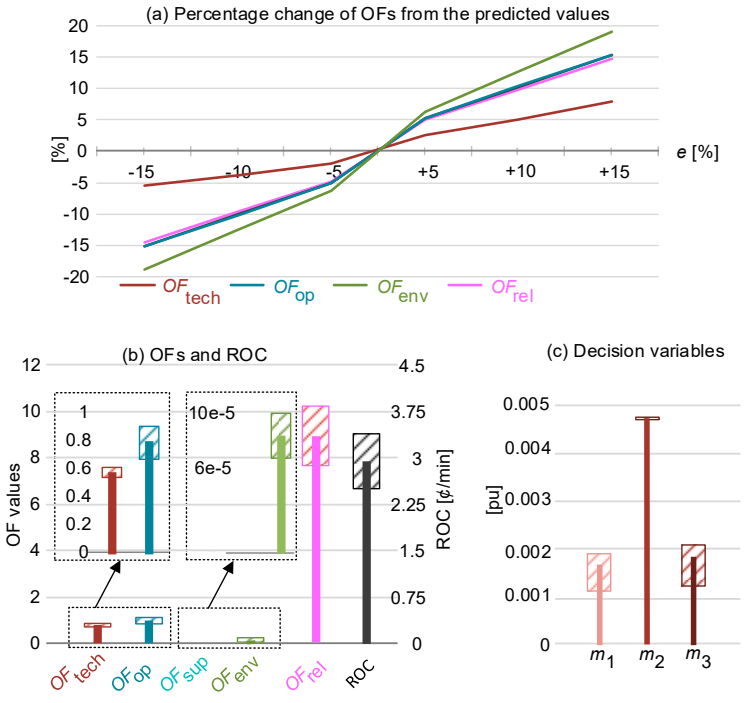

Figure 9. (**a**) Changes in the actual value of each OF of (3) versus e; (**b**) the value of each OF and ROC for no error and the range of change for $-15\% < e < 15\%$; (**c**) the defined optimal control variables (i.e., the droop coefficient of DDGs) for no prediction error and its variation by re-analyzing the MG for the actual loads.

5.2. Prediction MAAPE ($\bar{e}$)

To illustrate the impact of $\bar{e}$ within the assumed scenarios of Table 2, used in the OF of (2), another study is conducted in which $\bar{e}$ changes from 0 to 15%. Figure 10a illustrates the range of variation for each OF of (3) versus the change in $\bar{e}$ for a sample VF violating event, for which the proposed PVFC is activated to prevent the violation. The total demand and the NDDG's outcome are predicted as 1.048 pu and 0.06 pu, respectively. Figure 10b depicts the number of supportive actions (by DR and BES) decided by the PVFC. It can be seen from this figure that the proposed PVFC has taken more conservative measures and chooses more expensive supportive actions (such as DR and BES) with an increase in $\bar{e}$ to guarantee that the VF of the MG will be retained within the *Desired region*. It is also seen that the ROC of the MG will be least if a very accurate forecasting tool (i.e., $\bar{e} = 0$) is used. Table 6 also shows the correlation indices for the OFs and the MG's ROC with $\bar{e}$. As seen from this table, all parameters have a linear correlation; however, some of them have a positive correlation (i.e., for OF_{sup} and ROC) while for the others, it is negative.

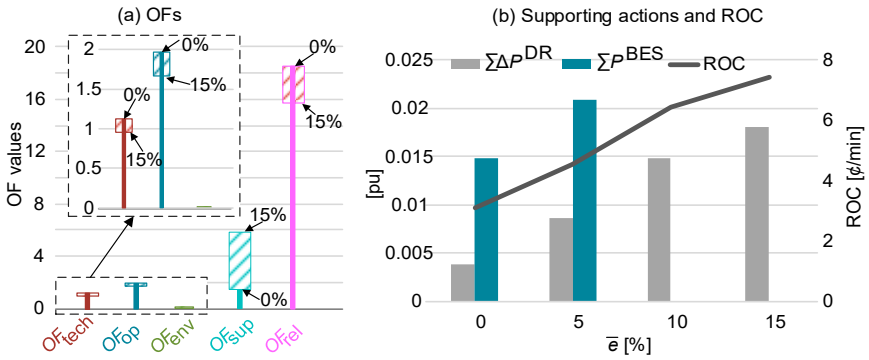

Figure 10. Sensitivity analysis result for changing $\bar{e}$ from 0 to 15% in Table 2: (**a**) changes in OFs; (**b**) changes in the contribution required from supportive actions and the MG's ROC.

Table 7 compares the FDI and VDI of the considered MG for an $\bar{e}$ of 0 and 15% for nine sample events. These events consequently correspond to the scenarios given in Table 2, in which it is assumed that $e = 15\%$. From this table, it can be seen that if $\bar{e}$ is ignored (i.e., $\bar{e} = 0$), the control variables defined by the PVFC cannot retain the VF within the *Desired region* for some of these sample events. However, the MG's FDI and VDI are within the acceptable limit for all considered sample events for $\bar{e}$ =15%.

Table 7. MG's VDI and FDI under few sample events assuming $\bar{e}$ is 0 or 15%.

$\bar{e}$ (%)	0		15	
Event	***FDI* (Hz)**	***VDI* (pu)**	***FDI* (Hz)**	***VDI* (pu)**
1	0.465	0.0475	0.355	0.0238
2	#		0.465	0.0306
3	0.315	0.014	0.245	0.0173
4	#		0.485	0.048
5	0.295	0.0135	0.23	0.0167
6	#		0.475	0.0406
7	0.305	0.0138	0.24	0.017
8	0.455	0.0392	0.35	0.0235
9	#		0.365	0.0241

Unacceptable VF deviation.

5.3. Scenario Probability (π^s)

In all the previous numerical analyses, the same probability was assumed for the scenarios of Table 2 ($\pi^1 = \ldots = \pi^9$). To illustrate the impact of π^s, another study is conducted for the example of Section 4.2. In this study, the probability of scenario 1 (i.e., π^1) is varied from 0.2 to 0.8 in steps of 0.2 while the rest of the scenarios in Table 2 have an equal probability. Figure 11 illustrates the result of this study for the different OFs of (3), as well as the MG's ROC, for each analysis. It can be seen from this figure that the proposed PVFC is not affected by the variations in the probability of the scenarios and π^s is less dominant than e, which is also evident from the correlation indices of Table 6.

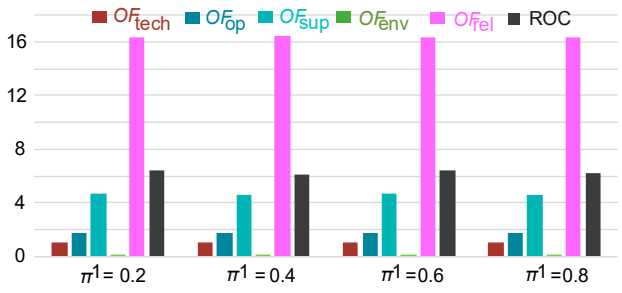

Figure 11. Sensitivity analysis result for changes in π^1 from 0.2 to 0.8.

6. Conclusions

An effective preventive control technique is proposed in this paper that uses the short-horizon prediction data of demand and NDDG's generation. It aims to determine the most optimal control actions for a standalone MG at the least cost and prevent the deviation of the VF of the MG beyond the *Desired region*. The proposed technique defines the most optimal droop coefficient settings for the DDGs and the level of engagement of BES, DR and RC, along with external support from an NMG and MG reconfiguration. Numerical analyses demonstrate that the proposed method ensures that the MG always operates within the expected VF range. Furthermore, it benefits the MG by minimizing the operation costs along with improving its technical, environmental and reliability aspects. The MG operator can prioritize these aspects, according to their policies or performance indices. The studies illustrate that the proposed controller will be able to retain the VF of the MG within the *Desired region* as far as the prediction error is acceptable. The studies also show

that by considering a more substantial prediction error, the proposed technique will take more conservative actions. Thus, using prediction tools that have a smaller error will result in the MG's more optimal performance.

It should be noted that as a very short-horizon preventive approach, the proposed PVFC is limited by the calculation time. Hence, using fast processors, simplified PFA tools and enhanced optimization solvers is essential when employing the proposed PVFC for very large MGs that have a very large number of control variables.

Author Contributions: Conceptualization, M.A.S. and F.S.; methodology, M.A.S. and F.S.; validation, M.A.S.; writing—original draft preparation, F.S.; writing—review and editing, F.S., G.S. and F.W.; supervision, F.S. and G.S. All authors have read and agreed to the published version of the manuscript.

Funding: This research received no external funding.

Data Availability Statement: Data is unavailable due to privacy restrictions.

Conflicts of Interest: The authors declare no conflict of interest.

Nomenclature

BES	Battery energy storage
DR	Demand response
DG	Distributed generation unit
DDG	Dispatchable DG
MAAPE	Mean arctangent absolute percentage error
MG	Microgrid
MGCC	MG's central controller
MPSO	Modified particle swarm optimization
NMGs	Neighboring MGs
NDDG	Non-dispatchable DG
OF	Objective function
pu	Per-unit
PFA	Power flow analysis
PVFC	Preventive VF controller
ROC	Real operating cost
RL	Reconfigurable line
RC	Renewable curtailment
SR	Spinning reserve
VF	Voltage or frequency

Appendix A. Provisionally Coupled Neighboring MGs

It is assumed that in the near future, with the incentives provided by governments in light of their renewable energy or greenhouse gas reduction targets, many private investors will be interested in building up and operating their own MGs. As such, the MG operator would prefer to operate its network in the standalone mode under normal operating conditions to maintain its autonomy. Thus, each MG can be owned or operated by different entities and under various operational standards and policies. With all careful design and operational planning, it may be unavoidable for an MG to experience unacceptable VF violations due to the imbalance between demand and generation. Hence, the concept of provisional MGs is proposed in [45–55], which allows standalone MGs to temporarily couple to suitable islanded NMGs, if available, to support each other by exchanging power, under abnormal conditions (i.e., emergencies such as overloading or over-generation).

Appendix B. Employed Optimization Solver

An MPSO-based solver is used in this study to solve the optimization problem of (2). Since MPSO is a metaheuristic approach and uses random numbers as the inputs of the optimization, this solver does not necessarily yield the same result if it re-runs multiple times for the same study case. Nevertheless, its outcome in each run should be near the

average value of all runs. To demonstrate this, the MPSO is re-run 100 times for the first event of Figure 6 (i.e., t = 13 min). Figure A1a,b depicts the probability and cumulative density functions for the least OF (i.e., the best solution in each run). This figure shows that in 80% of the runs, the defined least OF is near the average value of the runs. In addition, Figure A1c shows the convergence of MPSO for a sample run.

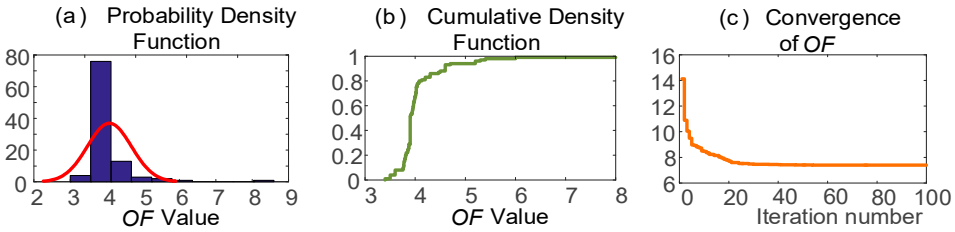

Figure A1. (**a**) Probability density function and (**b**) cumulative density function of 100 runs of MPSO. (**c**) MPSO's convergence over iterations in one sample run.

Appendix C. Employed Power Flow Analysis

Due to the lack of a slack bus, unlike conventional power systems, the frequency in an islanded MG is not constant and varies around the nominal value according to the DDGs, based on their droop Equation (1a). Hence, conventional PFA techniques cannot be employed for islanded MGs, and modified approaches, such as that proposed in [42], are required, which can also calculate frequency. In this study, the PFA introduced in [42] has been used within the developed PVFC to determine the MG's frequency, power loss and the voltage magnitudes at its buses at each stage of optimization. This load flow and optimization technique are developed in MATLAB via coding. To demonstrate the accuracy of the developed load flow technique, which is the core of the optimization in this study (as seen from the flowchart of Figure 2), a comparative analysis is undertaken between the PFA results realized in MATLAB for the sample six-bus network of [42] with those results when realized in PSCAD/EMTDC. The comparison showed a maximum deviation of 0.01% for voltage magnitudes and a maximum of 0.34% for the voltage angles of the buses, which consequently yields a maximum of 0.12% deviation in the powers of all lines, loads and sources, and validates the accuracy of the employed PFA function.

Table A1. Considered technical parameters for the MG in Figure 5.

MG's DDGs	DDG-1	DDG-2	DDG-3	Costs		
α_{DDG} (%)	10	10	0	$\left(Cost^{trade}\right)^{imp}$	0.3	($/kWh)
$\left(P^{DDG}\right)^{max}$ (kW)	7	7	7	$\left(Cost^{trade}\right)^{exp}$	0.3	($/kWh)
$\left(T_{DDG}\right)^{off}$ (min)	5	5	0.5	$Cost^{loss}$	0.04	($/kWh)
$\left(T_{DDG}\right)^{on}$ (min)	15	15	0.5	$Cost^{RC}$	25	($/kWh)
$\left(RR^{max}_{DDG}\right)^{up}$ (kW/s)	10	10	60	$Cost^{em}$	0.037	($/kg)
$\left(RR^{max}_{DDG}\right)^{down}$ (kW/s)	10	10	60	$Cost^{ENS}$	20	($/kWh)
$fuel$ (L/kWh)	0.2	0.25		$\left(Cost^{DR}\right)^{shed}$	3	($/kWh)
C^{fuel} ($/L)	0.8	1		$\left(Cost^{DR}\right)^{add}$	2	($/kWh)
$C^{O\&M}$ ($/h)	0.05	0.05	0.01	C^{BES}_{cap}	800	($/kWh)
C^{DG}_{cap} ($/kW)	400	500	700	$Cost^{sw}$	0.1	($/switching)
T^{op} (h)	12,000	15,000				
Em^{DG} (kg/kWh)	0	0.014	0			
$Cost^{ST}$ ($)	7	8	0			

Av_{NDDG} = 0.7; Av_{BES} = 0.9; Av_{EE} = 0.85; Av_{DDG-1} = 0.85; Av_{DDG-2} = 0.85; Av_{DDG-3} = 0.7; E^{life} = 1950 kWh; I^{max} = 25 A; SRI^{max} = 0.9; RCI^{max} = 0.4; EDI^{max} = 0.2; P^{max}_{loss} = 10% of load; ω_1 = 0.1; ω_2 = 0.3; ω_3 = 0.3; ω_4 = 0.1; ω_5 = 0.2; α^{RC} = 50%; α^{add} = 30%; α^{shed} = 50%; $V_{base} = V_{nom}$ = 220 V; S_{base} = 20 kVA; $f_{base} = f_{nom}$ = 50 Hz.

Table A2. Considered technical parameters for MG in Figure A2.

MG's DDGs	DDG-1,2	DDG-3,4	DDG-5,6	MG's DDGs	DDG-1,2	DDG-3,4	DDG-5,6
α_{DDG} (%)	10	10	0	C^{fuel} (\$/L)	0.8	1	
$(P^{DDG})^{max}$ (MW)	1.5	1.5	1.5	$C^{O\&M}$ (\$/h)	0.08	0.08	0.04
$(T_{DDG})^{off}$ (min)	10	10	0.5	C^{DG}_{cap} (\$/kW)	400	500	700
$(T_{DDG})^{on}$ (min)	15	15	0.5	T^{op} (h)	12,000	15,000	
$(RR^{max}_{DDG})^{up}$ (kW/s)	10	10	60	Em^{DG} (kg/kWh)	0	0.014	0
$(RR^{max}_{DDG})^{down}$ (kW/s)	10	10	60	$Cost^{ST}$ (\$)	10	10	0
fuel (L/kWh)	0.2	0.25					

Av_{NDDG} = 0.8; Av_{BES} = 0.9; Av_{EE} = 0.85; $Av_{DDG-1,2}$ = 0.9; $Av_{DDG-3,4}$ = 0.9; $Av_{DDG-5,6}$ = 0.8; E^{life} = 1950 kWh; I^{max} = 35 A; SRI^{max} = 0.9; RCI^{max} = 0.6; EDI^{max} = 0.1; P^{max}_{loss} = 10% of load; ω_1 = 0.1; ω_2 = 0.3; ω_3 = 0.3; ω_4 = 0.1; ω_5 = 0.2; α^{RC} = 50%; α^{add} = 30%; α^{shed} = 50%; $V_{base} = V_{nom}$ = 11 kV; S_{base} = 1.5 MVA; $f_{base} = f_{nom}$ = 50 Hz.

Appendix D. Assumed Technical Parameters, Variables and Costs

The considered technical parameters and the assumed costs, weightings and coefficients in the numerical analyses of Sections 4 and 5 are provided in Table A1.

Appendix E. PVFC's Performance in Large MGs

To demonstrate the application of the proposed PVFC in a large MG, the 64-bus medium voltage system of Figure A2 is considered, which is an expansion of the network in Figure 5. The assumed cost values are the same as those given in Table A1, while Table A2 presents the considered technical parameters and coefficients for this network. The operation of the considered MG is analyzed for an assumed variation in its demand and NDDGs, over a sample 60-min period, as shown in Figure A3a. At t = 10 min, an undesired frequency rise is predicted for t = 15 min (see Figure A3b). As such, the PVFC takes action and adjusts the control variables accordingly to prevent the frequency violation. Likewise, at t = 34 min, another VF violating event is predicted for t = 39 min. Again, the PVFC successfully takes action and prevents this prospective violation, as depicted in Figure A3b–c. As expected, the PVFC satisfies all technical constraints (i.e., *SRI*, *RCI*, *EDI*) by keeping them below the maximum acceptable limit in both events. This example can illustrate the successful operation of the proposed PVFC even for MGs with larger networks and a large number of distributed loads.

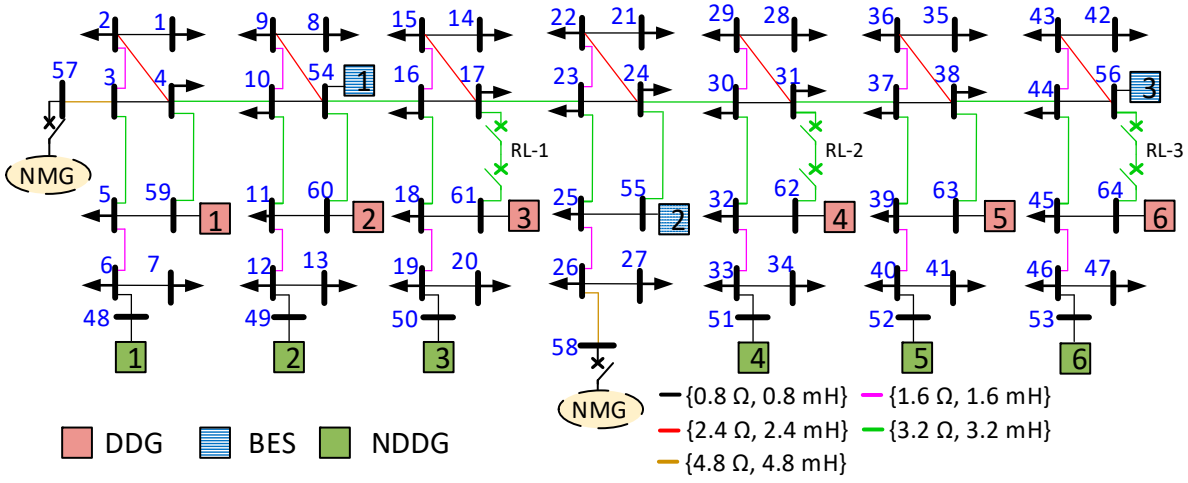

Figure A2. Considered 64-bus MG.

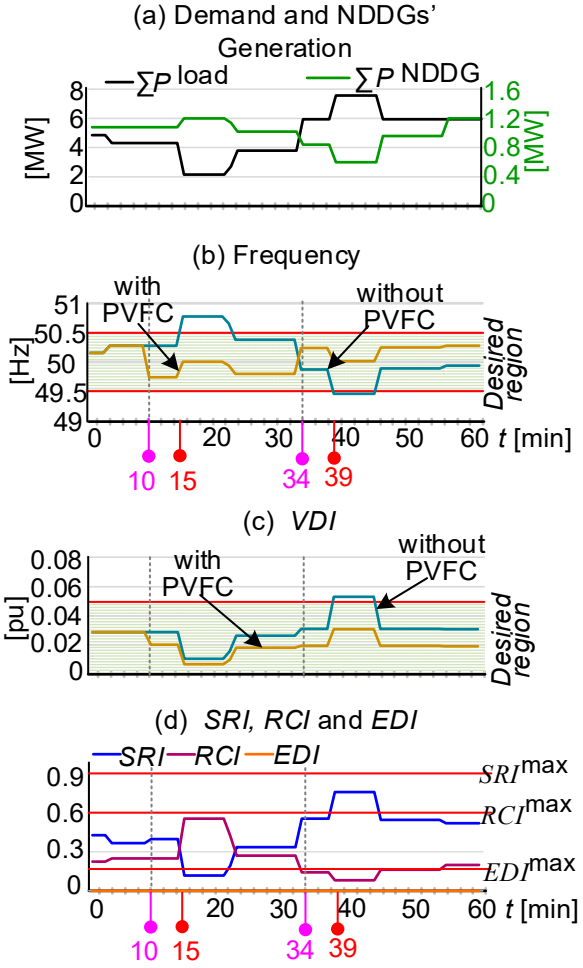

Figure A3. Performance of the proposed PVFC for the 64-bus MG.

Appendix F. PVFC's Time Complexity

The complexity of the optimization problem increases as the number of decision variables (i.e., the number of BESs, DDGs, NDGs, loads, etc.) increases. As such, this complexity increase is in line with an increase in the number of buses of the network to which these components are connected. Furthermore, as the number of buses increases, the PFA calculations within each stage of the optimization solution become more time-consuming. Therefore, another study is conducted to demonstrate the impact of the increasing size of the MG (i.e., its number of buses) on the proposed PVFC. Table A3 lists seven systems, in which the number of buses of the assumed MG of Figure 5 increases from 9 to 63. The total number of decision variables in these systems also increases from 17 to 95. As multiple PFA iterations take place inside each PSO iteration, the number of PFA iterations is considered as the basic operation. The total number of operations is monitored when the proposed technique is applied to each of these systems. Figure A4 depicts this relationship and shows a logarithmic time complexity (denoted by $O(log\ n)$) for the proposed PVFC [56]. Hence, the operation time of the proposed technique increases as the size and number of decision variables of the system becomes bigger. However, it is noteworthy that, with the ongoing advancements in industrial and real-time processors, it is expected that there will be access to superfast platforms that satisfy the required processing speed even for extremely large MGs in the near future.

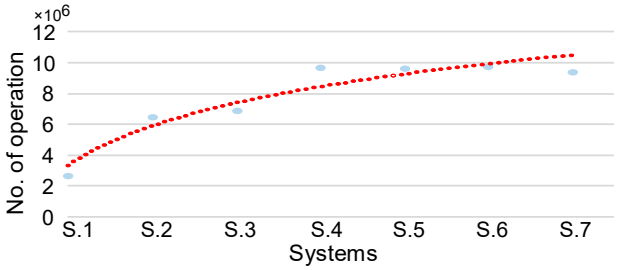

Figure A4. The time complexity of the proposed technique.

Table A3. Systems considered for the time complexity analysis.

System	S.1	S.2	S.3	S.4	S.5	S.6	S.7
Number of buses	9	18	27	36	45	54	63
Number of decision variables	17	30	43	56	69	82	95

References

1. Lasseter, R.H. Microgrids. *IEEE PES Winter Meet.* **2002**, *1*, 305–308.
2. Majzoobi, A.; Khodaei, A. Application of microgrids in supporting distribution grid flexibility. *IEEE Trans. Power Syst.* **2017**, *32*, 3660–3669. [CrossRef]
3. Khuntia, S.R.; Rueda, J.L.; van der Meijden, M.A.M.M. Neural network-based load forecasting and error. In Proceedings of the 2016 International Joint Conference on Neural Networks (IJCNN), Vancouver, BC, Canada, 24–29 July 2016; pp. 4970–4975.
4. Liu, N.; Tang, Q.; Zhang, J.; Fan, W.; Liu, J. A hybrid forecasting model with parameter optimization for short-term load forecasting of micro-grids. *Appl. Energy* **2014**, *129*, 336–345. [CrossRef]
5. Hernandez, L.; Baladron, C.; Aguiar, J.M.; Carro, B.; Sánchez-Esguevillas, A.; Lloret, J. Artificial neural networks for short-term load forecasting in microgrids environment. *Energy* **2014**, *75*, 252–264. [CrossRef]
6. Coelho, V.N.; Coelho, I.M.; Coelho, B.N.; Reis, A.J.; Enayatifar, R.; Souza, M.J.; Guimarães, F.G. A self-adaptive evolutionary fuzzy model for load forecasting problems on smart grid environment. *Appl. Energy* **2016**, *169*, 567–584. [CrossRef]
7. Saez, D.; Avila, F.; Olivares, D.; Canizares, C.; Marin, L. Fuzzy prediction interval models for forecasting renewable resources and loads in microgrids. *IEEE Trans. Smart Grid* **2015**, *6*, 548–556. [CrossRef]
8. Wan, C.; Zhao, J.; Song, Y.; Xu, Z.; Lin, J.; Hu, Z. Photovoltaic and solar power forecasting for smart grid energy management. *CSEE J. Power Energy Sys.* **2015**, *1*, 38–46. [CrossRef]
9. Buhan, S.; Cadırcı, I. Multistage Wind-electric power forecast by using a combination of advanced statistical methods. *IEEE Trans. Ind. Inform.* **2015**, *11*, 1231–1242. [CrossRef]
10. Xie, L.; Gu, Y.; Zhu, X.; Genton, M.G. Short-term spatio-temporal wind power forecast in robust look-ahead power system dispatch. *IEEE Trans. Smart Grid* **2014**, *5*, 511–520. [CrossRef]
11. Genikomsakis, K.; Lopez, S.; Dallas, P.I.; Ioakimidis, C.S. Simulation of wind-battery microgrid based on short-term wind power forecasting. *Appl. Sci.* **2017**, *7*, 1142. [CrossRef]
12. Liu, J.; Fang, W.; Zhang, X.; Yang, C. An improved photovoltaic power forecasting model with the assistance of aerosol data. *IEEE Trans. Sust. Energy* **2015**, *6*, 434–442. [CrossRef]
13. Anagnostos, D.; Schmidt, T.; Cavadias, S.; Soudris, D.; Poortmans, J.; Catthoor, F. A method for detailed, short-term energy yield forecasting of photovoltaic installations. *Renew. Energy* **2019**, *130*, 122–129. [CrossRef]
14. Olivares, D.E.; Mehrizi-Sani, A.; Etemadi, A.H.; Canizares, C.A.; Iravani, R.; Kazerani, M.; Hajimiragha, A.H.; Gomis-Bellmunt, O.; Saeedifard, M.; Palma-Behnke, R.; et al. Trends in Microgrid Control. *IEEE Trans. Smart Grid* **2014**, *5*, 1905–1919. [CrossRef]
15. Sanjari, M.J.; Gharehpetian, G.B. Unified framework for frequency and voltage control of autonomous microgrids. *IET Gener. Transm. Distrib.* **2013**, *7*, 965–972. [CrossRef]
16. Anvari-Moghadam, A.; Shafiee, Q.; Vasquez, J.C.; Guerrero, J.M. Optimal adaptive droop control for effective load sharing in ac microgrids. In Proceedings of the IECON 2016—42nd Annual Conference of the IEEE Industrial Electronics Society, Florence, Italy, 23–26 October 2016.
17. Moradi, M.H.; Abedini, M.; Hosseinian, S.M. Optimal operation of autonomous microgrid using HS-GA. *Int. J. Electr. Power Energy Syst.* **2016**, *77*, 210–220. [CrossRef]
18. Nourollah, S.; Aminifar, F.; Gharehpetian, G.B. A hierarchical regionalization-based load shedding plan to recover frequency and voltage in microgrid. *IEEE Trans. Smart Grid.* **2018**, *10*, 3818–3827. [CrossRef]
19. Dong, Y.; Xie, X.; Shi, W.; Zhou, B.; Jiang, Q. Demand-response based distributed preventive control to improve short-term voltage stability. *IEEE Trans. Smart Grid.* **2017**, *9*, 4785–4795. [CrossRef]

20. Olivares, D.E.; Canizares, C.A.; Kazerani, M. A centralized energy management system for isolated microgrids. *IEEE Trans. Smart Grid* **2014**, *5*, 1864–1875. [CrossRef]
21. Wu, Y.; Ye, G.; Tang, K.-T. Preventive control strategy for an island power system that considers system security and economics. *IEEE Trans. Ind. Appl.* **2017**, *53*, 5239–5251. [CrossRef]
22. Han, Y.; Li, H.; Shen, P.; Coelho, E.A.A.; Guerrero, J.M. Review of active and reactive power sharing strategies in hierarchical microgrids. *IEEE Trans. Power Electron.* **2017**, *32*, 2427–2451. [CrossRef]
23. Hossain, M.A.; Pota, H.R.; Hossain, M.J.; Blaabjerg, F. Evolution of microgrids with converter-interfaced generations: Challenges and opportunities. *Int. J. Electr. Power Energy Syst.* **2019**, *109*, 160–186. [CrossRef]
24. Valle, Y.D.; Venayagamoorthy, G.K.; Mohagheghi, S.; Hernandez, J.-C.; Harley, R.G. Particle swarm optimization: Basic concepts, variants and applications in power systems. *IEEE Trans. Evol. Comput.* **2008**, *12*, 171–195. [CrossRef]
25. Eberhart, R.C.; Shi, Y. *Particle Swarm Optimization: Developments, Applications and Resources*; Congress on Evolutionary Computation: Seoul, Republic of Korea, 2001.
26. Networks, W. ABB. 2019. Available online: https://global.abb/group/en (accessed on 1 July 2023).
27. Communication, I.W. Siemens. 2019. Available online: http://w3.siemens.com/mcms/automation/en/industrial-communications/industrial-wireless-communication/pages/industrial-wireless-communication.aspx (accessed on 1 July 2023).
28. Mean Time Between Failures (MTBF), Siemens. 2019. Available online: https://support.industry.siemens.com/cs/document/109479200/mean-time-between-failures-(mtbf)-%e2%80%93-list-for-ruggedcom-products?dti=0&pnid=16008&lc=en-af (accessed on 1 July 2023).
29. Kim, S.; Kim, H. A new metric of absolute percentage error for intermittent demand forecasts. *Int. J. Forecast.* **2016**, *32*, 669–679. [CrossRef]
30. Zhao, B.; Zhang, X.; Chen, J.; Wang, C.; Guo, L. Operation optimization of standalone microgrids considering lifetime characteristics of battery energy storage system. *IEEE Trans. Sustain. Energy* **2013**, *4*, 934–943. [CrossRef]
31. Merei, G.; Berger, C.; Sauer, D.U. Optimization of an off-grid hybrid PV-wind-diesel system with different battery technologies using genetic algorithm. *Sol. Energy* **2013**, *97*, 460–473. [CrossRef]
32. Kariuki, K.; Allan, R.N. Evaluation of reliability worth and value of lost load. *IEE Gener. Transm. Distrib.* **1996**, *143*, 171–180. [CrossRef]
33. Wang, M.Q.; Gooi, H.B. Spinning reserve estimation in microgrids. *IEEE Trans. Power Syst.* **2011**, *26*, 1164–1174. [CrossRef]
34. Hummon, M. *Value of Demand Response: Quantities from Production Cost Modeling*; Technical Report, NREL/PR-6A20-61815; National Renewable Energy Laboratory: Golden, CO, USA, 2014.
35. Luckow, P.; Stanton, E.A.; Fields, S.; Biewald, B.; Jackson, S.; Fisher, J.; Wilson, R. *Carbon Dioxide Price Forecast*; Technical Report; Synapse Energy Economics: Cambridge, MA, USA, 2014.
36. Shoeb, M.A.; Shafiullah, G. Renewable energy integrated islanded microgrid for sustainable irrigation—A Bangladesh perspective. *Energies* **2018**, *11*, 1283. [CrossRef]
37. Bird, L.; Cochran, J.; Wang, X. *Wind and Solar Energy Curtailment: Experience and Practices in the United States*; Technical Report, NREL/TP-6A20-60983; National Renewable Energy Laboratory: Golden, CO, USA, 2014.
38. Feinberg, E.A.; Hu, J.; Huang, K. A rolling horizon approach to distribution feeder reconfiguration with switching costs. In Proceedings of the 2011 IEEE International Conference on Smart Grid Communications (SmartGridComm), Brussels, Belgium, 17–20 October 2011.
39. Billinton, R. *Power System Reliability Evaluation*; Taylor & Francis: Abingdon, UK, 1970.
40. Xu, Y.; Zhang, W.; Liu, W. Distributed dynamic programming-based approach for economic dispatch in smart grids. *IEEE Trans. Ind. Inform.* **2015**, *11*, 166–175. [CrossRef]
41. Shahnia, F.; Bourbour, S.; Ghosh, A. Coupling neighboring microgrids for overload management based on dynamic multicriteria decision-making. *IEEE Trans. Smart Grid* **2017**, *8*, 969–983. [CrossRef]
42. Mumtaz, F.; Syed, M.H.; Al Hosani, M.; Zeineldin, H.H. A novel approach to solve power flow for islanded microgrids using modified newton raphson with droop control of DG. *IEEE Trans. Sustain. Energy* **2016**, *7*, 493–503. [CrossRef]
43. Shoeb, M.; Shahnia, F.; Shafiullah, G. A multilayer preventive control to regulate voltage and frequency in autonomous microgrids. In Proceedings of the 2018 Australasian Universities Power Engineering Conference (AUPEC), Auckland, New Zealand, 27–30 November 2018.
44. Shoeb, M.; Shahnia, F.; Shafiullah, G.; Su, X. Sensitivity of prediction error on the performance of a preventive controller for microgrids. In Proceedings of the 2019 IEEE International Conference on Industrial Technology (ICIT), Melbourne, Australia, 13–15 February 2019.
45. Shoeb, M.; Shahnia, F.; Shafiullah, G. A multilayer and event-triggered voltage and frequency management technique for microgrid's central controller considering operational and sustainability aspects. *IEEE Trans. Smart Grid* **2019**, *10*, 5136–5151. [CrossRef]
46. Shoeb, M.; Shahnia, F.; Shafiullah, G. Peer-to-peer load allocation using potential field concept for optimal operation of standalone microgrids. *IET Gener. Transm. Distrib.* **2020**, *14*, 6061–6070. [CrossRef]
47. Khodaei, A. Provisional microgrids. *IEEE Trans. Smart. Grid* **2015**, *6*, 1107–1115. [CrossRef]
48. Ferdous, S.; Shahnia, F.; Shafiullah, G. Provisional energy transaction management amongst neighbouring microgrids through a dc power exchange link. *IET Power Electron.* **2020**, *13*, 4129–4139. [CrossRef]

49. Ferdous, S.; Shahnia, F.; Shafiullah, G. Stability and robustness of a coupled microgrid cluster formed by various coupling structures. *Chin. J. Electr. Eng.* **2021**, *7*, 60–77. [CrossRef]
50. Lasseter, R.H. Smart distribution: Coupled microgrids. *Proc. IEEE* **2011**, *99*, 1074–1082. [CrossRef]
51. Ferdous, S.; Shahnia, F.; Shafiullah, G. Power sharing and control strategy for provisionally coupled microgrid clusters through an isolated power exchange network. *Energies* **2021**, *14*, 7514. [CrossRef]
52. Ferdous, S.; Shahnia, F.; Shafiullah, G. Realising a system of coupled microgrid networks using single-phase interconnection lines. *IET Smart Grid* **2021**, *4*, 346–364. [CrossRef]
53. Pashajavid, E.; Shahnia, F.; Ghosh, A. Provisional internal and external power exchange to support remote sustainable microgrids in the course of power deficiency. *IET Gen. Trans. Dist.* **2017**, *11*, 246–260. [CrossRef]
54. Ferdous, S.; Shafiullah, G.; Shahnia, F.; Elavarasan, R.; Subramaniam, U. Dynamic frequency and overload management in autonomous coupled microgrids for self-healing and resiliency improvement. *IEEE Access* **2020**, *8*, 116796–116811. [CrossRef]
55. Shoeb, M.; Shafiullah, G.; Shahnia, F. Coupling adjacent microgrids and cluster formation under a look-ahead approach reassuring optimal operation and satisfactory voltage and frequency. *IEEE Access* **2021**, *9*, 78083–78097. [CrossRef]
56. Sipser, M. *Introduction to the Theory of Computation*; Cengage Learning: Boston, MA, USA, 2012.